Chemical Engineering Journal 486 (2024) 150339

Contents lists available at ScienceDirect

Chemical Engineering Journal

journal homepage: www.elsevier.com/locate/cej

Enhanced catalytic activity of H_2 heat-treated porous ceria for direct conversion of carbon dioxide into dimethyl carbonate

Zhuxian Yang [a], Monica Mengdie Lin [b], Xinhuan Lu [c], Justin Tay Zheng [b], Wen-Yueh Yu [b,*], Yanqiu Zhu [a], Hong Chang [a], Yongde Xia [a,*]

[a] Department of Engineering, Faculty of Environment, Science and Economy, University of Exeter, Exeter, EX4 4QF, United Kingdom
[b] Department of Chemical Engineering, National Taiwan University, No.1, Sec. 4 Roosevelt Rd. Taipei, Taiwan, 106335 Taiwan
[c] School of Chemistry and Chemical Engineering, Hubei University, 368 Youyi Dadao, Wuchang Qu, Wuhan, Hubei Province, 430062, PR China

ARTICLE INFO

Keywords:
Dimethyl carbonate
Ceria
Heat treatment
Carbon dioxide
Surface defects

ABSTRACT

It has been demonstrated that the specific surface area, acid–base properties, morphologies, and oxygen-vacancies (O_v) play a role in the catalytic performance of CeO_2-based catalysts. In this study, porous CeO_2 and Zr-doped CeO_2 catalysts with high surface area have been prepared via a low temperature synthesis strategy and evaluated for the conversion of CO_2 and methanol into dimethyl carbonate (DMC). Results show that the Zr doping (Zr:Ce = 1:9) could slightly increase the DMC formation rate of CeO_2, whereas the H_2 heat-treatment of CeO_2 could lead to a DMC formation rate of 18.22 ± 0.64 mmol $g^{-1}h^{-1}$, which is amongst the highest for CeO_2 catalysts at 140 °C reported so far. Such enhancement in DMC formation rate is attributed to (1) the balanced crystallinity and defects of the CeO_2, (2) a shift of acid and base activity to lower temperature, and (3) the (1 1 1) plane only surface termination of the catalyst resulted from the heat-treatment process. Excluding the best performed H_2 heat-treated CeO_2 catalyst, the DMC formation rate of the rest catalysts shows a positive link to the BET surface area, acid property (NH_3-TPD), O_V%, Ce^{3+}%, and the Raman peak intensity ratio of I_D/I_{F2g} of the catalyst. The low temperature preparation strategy in this study could be applicable to the synthesis of CeO_2 catalyst towards other reactions (*e.g.*, non-reductive CO_2 conversions to various carbonates, carbamates, urea derivatives, etc.).

1. Introduction

Dimethyl carbonate (DMC) is a very important compound due to its versatile properties and corresponding applications. For example, because of its low toxicity, low viscosity, good dissolving ability as well as its carbonyl group and methyl group containing nature, it can be used as replacement for toxic and hazardous materials (*e.g.*, phosgene, dimethyl sulfate, etc.), and in carbonylation and methylation reactions [1,2]. In addition, its high oxygen content (53 %) and octane number (1 0 5) make it a potential additive to fuel oil [3,4].

Industrialized processes for DMC production include phosgenation [5], transesterification [6,7], liquid phase methanol oxidative carbonylation [8,9], and vapor-phase methyl nitrite carbonylation [10,11]. However, the phosgenation process has been discontinued because it involves the use of hypertoxic phosgene and the other processes suffer from problems such as high cost, explosion risk [11]. Therefore, it is highly desirable to develop environmentally friendly and cost-effective methods for DMC production. Methods including direct DMC synthesis from carbon dioxide (CO_2) and methanol (MeOH) [12], transesterification of ethylene carbonate (EC) and MeOH [13], and transesterification of urea and MeOH [14] have been studied for DMC production, among which the direct DMC synthesis from CO_2 and MeOH based on the following equation has attracted much attention because it can not only avoid the generation of toxic product, but also turn the greenhouse gas, CO_2, into the value-added product, DMC.

$$CO_2 + 2CH_3OH \rightarrow (CH_3O)_2CO + H_2O$$

However, there are two issues with this reaction. One is that CO_2 is very stable, and a high amount of energy input is required to activate CO_2; the other is the unfavourable thermodynamic equilibrium of this reaction and dehydrating agents are needed to shift the equilibrium by eliminating the in situ produced water to increase the DMC yield [4,11,15,16]. Therefore, effective catalysts (to decrease the energy barrier), high CO_2 pressure and dehydrating agents (to shift the

* Corresponding authors.
E-mail addresses: wenyueh@ntu.edu.tw (W.-Y. Yu), y.xia@exeter.ac.uk (Y. Xia).

https://doi.org/10.1016/j.cej.2024.150339
Received 21 November 2023; Received in revised form 26 February 2024; Accepted 9 March 2024
Available online 11 March 2024

equilibrium) have been used to tackle these issues. Various dehydrating agents such as 2,2-dimethoxy propane (DMP) [17], molecular sieves 3A [18], and 1,1,1-trimethoxymethane (TMM) [19], Linde type A zeolites [16], hydrophilic LTA and SOD membranes [20], etc. have been studied to improve the DMC yield. Meanwhile, a number of catalysts including potassium carbonate [21], organometallic compounds [22], metal tetraalkoxides [23], V_2O_5 [24], Y_2O_3 [25], ZrO_2 [15,26–28], CeO_2 [12,29,30], etc. have been studied for direct DMC synthesis. Among them, the CeO_2 based catalysts are the most extensively studied ones due to their high catalytic activity [31].

It has been demonstrated that the specific surface area [12,32], the acid–base properties [15,33–37], morphologies [38,39], the oxygen-vacancies [29,40–42] of the CeO_2/CeO_2-based catalyst play a role in their catalytic performance [43–45]. For example, Yoshida et al. reported that the DMC formation rate of CeO_2 catalysts calcined at 600 °C and above was almost proportional to the BET surface area of catalysts [12]. Liu et al. showed that the acid–base properties and oxygen vacancies of the catalyst played a crucial role in promoting the formation of DMC [33]. Wang et al. showed that the spindle-like CeO_2 exhibited the highest DMC yield followed by nano-rods, nano-cubes and nano-octahedrons [38]. In addition, Yang et al. reported that the distinguished catalytic performance of the CeO_2 catalyst is attributed to the overall effect of the high surface area, surface defects and basic sites of the catalyst [45]. Kuan et al. reported that abundant Ce^{3+} and oxygen vacancy sites of the refluxing synthesized CeO_2 nanorod significantly promoted the DMC yield [29]. Therefore, various synthesis strategies have been explored to improve the catalytic performance, including creating porous structures, preparing CeO_2 with 1D nanostructures [29,41,46], doping metal cations (*e.g.*, Zr^{4+}, Ti^{4+}, Ca^{2+}, Mn^{2+}, Bi^{3+}, etc.) to the CeO_2 lattice to increase oxygen vacancies [17,33,34,40,46–49] and heat treating the catalysts in H_2 to promote oxygen vacancies [41,44].

Zr^{4+} has been the most studied doping cation to form CeO_2-ZrO_2 catalysts partly because ZrO_2 itself is an extensively investigated catalyst for direct DMC synthesis from CO_2 and MeOH [17,27,28,50–53]. It was reported that the Zr-doped CeO_2 nanorods exhibited significantly more oxygen vacancy sites than pure CeO_2 nanorods [40]. Among the various Zr-doped CeO_2 catalysts, the equimolar composition ($Ce_{0.5}Zr_{0.5}O_2$) were reported to show the maximum catalytic activity for direct DMC synthesis compared to pure oxides of CeO_2 and ZrO_2 [47,54].

It has been reported that H_2 heat-treatment of CeO_2 is effective in enriching surface oxygen vacancies and accordingly improving the catalytic activity of the catalysts. In particular, Wada et al. achieved 1.6 times increase in DMC synthesis rate by pre-treating CeO_2 in H_2 at 400 °C [44]. Zhou et al. reported that surface oxygen vacancies could be formed when the Ni/CeO_2 catalyst was prepared in H_2 at 380 °C [55]. However, Zhang et al. reported that reduction treatment at 450–800 °C reduced the DMC yield, although it could promote the conversion of Ce^{4+} to Ce^{3+} and improve the concentration of surface oxygen vacancies of CeO_2 [56]. On the other hand, Fu et al. demonstrated that pre-treatment of CeO_2 nanowire in H_2 could remarkably increase the acid/base sites of the catalyst and improve the catalytic performance [41].

In this work, we aim to investigate the effect of both Zr-doping and H_2 heat-treatment on the crystallinity, textural property, acid-bas property, defects and catalytic activity of the resulting porous CeO_2 and Zr-doped CeO_2 catalysts. The porous CeO_2 and Zr-doped CeO_2 with various nominal Zr:Ce molar ratios of 1:18, 1:9, 1:1 and 1:0.25 have been prepared by refluxing a mixture of terephthalic acid, ammonium cerium nitrate and zirconium chloride in dimethylformamide at 100 °C followed by low temperature calcination at 400 °C. The pure CeO_2 sample and the Zr-doped CeO_2 sample with Zr:Ce ratio of 1:9 were further undergone H_2 heat-treatment at 400 °C. The resulting samples were characterised by XRD, N_2 adsorption analysis at −196 °C, CO_2 adsorption analysis at 25 °C, NH_3 temperature-programmed desorption (NH_3-TPD), and CO_2-temperature-programmed desorption (CO_2-TPD) for acid and base sites, Raman, XPS, SEM and TEM. The catalytic activity towards the direct conversion of CO_2 and MeOH into DMC was evaluated at 5.0 MPa (at R.T.), 140 °C for 3 h. The highest so far DMC formation rate of 18.22 ± 0.64 mmol $g^{-1}h^{-1}$ at 140 °C was achieved for the H_2 heat-treated CeO_2 catalyst. The effect of Zr-doping, H_2 heat-treatment, surface area, surface acid-base properties, surface defects, Ce^{3+} content and oxygen vacancies on the catalytic activity have been discussed and an attempted explanation for the remarkable enhancement in DMC formation rate by H_2 heat-treatment of CeO_2 has been proposed. The DMC formation mechanism of the best performed H_2 heat-treated CeO_2 catalyst was investigated by in-situ diffuse reflectance infrared Fourier transform spectroscopy (DRIFTS).

2. Experimental

2.1. Materials

Terephthalic acid, dimethylformamide, ammonium cerium (IV) nitrate and zirconium chloride were purchased from Merk. Acetone was purchased from Fisher Scientific.

0.8885 g terephthalic acid ($C_8H_6O_4$) was dissolved in 30 mL dimethylformamide (DMF), and 2.9193 g ammonium cerium (IV) nitrate ($(NH_4)_2Ce(NO_3)_6$) was dissolved in 10 mL distilled water. The two solutions were then mixed under stirring and refluxed at 100 °C for 0.25 h or 5.5 h. After cooling, the solid products were separated by centrifugation and washed with DMF for 4 times followed by washing with acetone for 4 times. The washed products were dried in air overnight, followed by oven drying at 70 °C overnight to obtain **CeUiO-66** [57] (refluxing for 0.25 h) and the CeO_2 precursor (named as **P_CeO$_2$**) (refluxing for 5.5 h), respectively. Different amounts of zirconium chloride ($ZrCl_4$) according to Zr:Ce molar ratios of 1:18, 1:9, 1:1, 1:0.25 was added to prepare the Zr-doped CeO_2 precursors (named as **P_CeO$_2$-1T18**, **P_CeO$_2$-1T9**, **P_CeO$_2$-1T1** and **P_CeO$_2$-1T0.25**, respectively). Based on the TGA of the CeO_2 precursor (**P_CeO$_2$**), shown in Fig. S1, the precursor was completely converted to CeO_2 at 300 °C, therefore 400 °C was adopted for the calcination process to obtain CeO_2 or Zr-doped CeO_2 catalysts. Briefly, 1.5 g CeO_2 precursor or Zr-doped CeO_2 precursors were annealed in air at 400 °C with heating rate of 2 °C min^{-1} for 3 h to generate pure CeO_2 and Zr-doped CeO_2 with different Zr:Ce molar ratios, named as **CeO$_2$**, **CeO$_2$-1T18**, **CeO$_2$-1T9**, **CeO$_2$-1T1**, **CeO$_2$-1T0.25**, corresponding to pure CeO_2 and Zr-doped CeO_2 with nominal Zr:Ce molar ratios of 1:18, 1:9, 1:1, 1:0.25, respectively. The pure CeO_2 and the best performed Zr-doped CeO_2 catalysts were further heat-treated under H_2 flow. Briefly, 0.2 g sample in an alumina boat was placed in a tube furnace which was heated at 5 °C min^{-1} under Ar flow of 100 mL min^{-1}. When the temperature was 250 °C, H_2 flow of 100 mL min^{-1} was introduced and the Ar flow was adjusted to 200 mL min^{-1}, which was maintained at 400 °C for 1 h, then the H_2 flow was stopped, and the furnace was cooled down under Ar flow of 100 mL min^{-1}. All the catalysts were kept in glass vials that were stored in air.

2.2. Characterisation

X-ray diffraction (XRD) was measured with a Bruker D8 advanced X-ray diffractometer with Cu Kα X-ray source (λ = 0.15418 nm) at 40 kV and 40 mA. N_2 gas sorption analysis was carried out with a Quantachrome Autosorb-iQ gas analyser using conventional volumetric technique at −196 °C. Samples were outgassed under vacuum at 200 °C for 6 h prior to analysis. The surface area was calculated with Brunauer-Emmett-Teller (BET) method using adsorption data in the partial pressure (P/P_0) range of 0.05–0.2. Pore size distribution was calculated with density functional theory model with adsorption data. CO_2 gas sorption analysis was performed in the same way for N_2 gas sorption analysis except that the analysis temperature was 25 °C.

X-ray photoelectron spectroscopy (XPS) measurements were carried out with a Kratos Axis Ultra system with a monochromated Al Kr X-ray source operated at 10 mA emission current and 15 kV anode potential.

The XPS spectra were deconvoluted with CasaXPS software. Raman spectra were obtained with a Renishaw InVia Qontor at 532 nm laser. The in-situ FT-IR spectra were obtained with an infrared spectrometer (Thermal Scientific Nicolet iS50) equipped with a mercury-cadmium-telluride (MCT) detector and a diffuse reflectance infrared Fourier transform spectroscopy (DRIFTS) chamber (Harrick Praying Mantis™ HVC-DRP-5) [58–61]. The measurements were carried out as follows, the chamber was pre-treated at 200 °C for 20 min with Ar flow of 40 mL min^{-1}. After the chamber was cooled to 140 °C, the methanol in saturator was introduced to the chamber by Ar flow of 40 mL min^{-1}, and the catalyst was purged with Ar flow of 40 mL min^{-1} for 10 min, then the flow was switched to high-purity CO_2 gas (99.999+%) at 40 mL min^{-1} for 10 min. The DRIFTS spectra were averaged from 16 scans with a resolution of 4 cm^{-1}.

NH_3-TPD was performed with a Quantachrome Chemstar TPX. 100 mg sample was heated under He flow of 30 mL min^{-1} at 300 °C for 40 min to remove surface impurities, followed by cooling. When the temperature was down to 35 °C, a mixture of 5 % NH_3/He with flow rate of 30 mL min^{-1} was introduced for a period of 30 min for the NH_3 adsorption by the sample to take place. Then the sample was purged with nitrogen for 30 min to eliminate the physically adsorbed NH_3 before the desorption of NH_3 took place, which was measured under temperature programming with heating rate of 10 °C min^{-1} in the range of 50–780 °C. CO_2-TPD was also carried out with Quantachrome Chemstar TPX. The above procedure used for NH_3-TPD measurement was adopted for the CO_2-TPD measurement except that the probe gas NH_3 was replaced by CO_2 and the TPD was measured in the range of 50–700 °C. H_2-TPR was conducted with Quantachrome ChemStar. 100 mg sample was heated with a heating rate of 10 °C min^{-1} in 10 % H_2/Ar mixture gas from 30 °C to 200 °C, and held at 200 °C for 30 min. Then the sample was cooled down to 30 °C. Next the sample was heated from 30 °C to 650 °C in 10 % H_2/Ar mixture gas with a heating rate of 10 °C min^{-1} and was hold at 650 °C for 1 h.

2.3. Evaluation of catalytic activity towards CO_2 conversion

The catalytic activity towards CO_2 conversion was measured with a 100-mL Parr reactor [29,42]. In brief, 370 mmol of methanol and 10 mg of CeO_2 catalyst were loaded in the reactor, followed by introducing 5.0 MPa CO_2 at room temperature. The reactor was then heated to 140 °C under stirring and kept at 140 °C for 3 h. Afterwards, the product in the reactor was analysed by a gas chromatography equipped with a flame ion detector (Agilent 6890 N GC-FID) and a capillary column (Zebron ZB-WAX). A pre-determined amount of 1-propanol was applied to the system as the internal standard for the quantitative analysis. The formation rate of DMC was calculated by dividing the DMC amount obtained at a reaction time of 3 h (Fig. S2) by the mass of catalyst used.

3. Results and discussion

3.1. Structures, textural properties and morphologies

Fig. S3 shows the XRD patterns of the CeO_2 precursor (P_CeO_2) and the Zr-doped CeO_2 precursors with various Zr:Ce molar ratios, P_CeO_2-1T18 (1:18), P_CeO_2-1T9 (1:9), P_CeO_2-1T1 (1:1) and P_CeO_2-1T0.25 (1:0.25). For easy comparison the XRD pattern of CeUiO-66 is also included, which was prepared under the same conditions except that no $ZrCl_4$ was added and the refluxing duration was 0.25 h [57]. The precursor for pure CeO_2 (P_CeO_2) shows very strong peaks of both cerium formate ($Ce(CHO_2)_3$) and CeUiO-66, suggesting that P_CeO_2 is a mixture of ($Ce(CHO_2)_3$) and CeUiO-66. However, upon addition of $ZrCl_4$ into the preparation mixture, the resulting Zr-doped CeO_2 precursors only exhibit peaks corresponding to ($Ce(CHO_2)_3$), implying that the Zr-doped CeO_2 precursors has the crystalline structures of ($Ce(CHO_2)_3$). In addition, the intensity of the peaks corresponding to ($Ce(CHO_2)_3$) significantly decreases when the Zr:Ce is 1:0.25, showing that the addition of Zr adversely affects the crystalline structure when the Zr:Ce ratio is higher than 1:0.25.

The XRD pattens of pure CeO_2 and Zr-doped CeO_2 with different Zr:Ce molar ratios obtained *via* annealing of the CeO_2 precursor and Zr-doped CeO_2 precursors in air at 400 °C are presented in Fig. 1a. Peaks at 2θ = 28.4, 32.9, 47.4, 56.3, 59.2, 69.3, 76.7 and 79.0°, corresponding to the (111), (200), (220), (311), (222), (400), (331) and (420) planes of cubic CeO_2 appear for the pure CeO_2 sample. For the Zr-doped samples, CeO_2-1T18 and CeO_2-1T9, only the first four peaks at 2θ = 28.4, 32.9, 47.4, 56.3° can be observed. For sample CeO_2-1T1, in addition to the aforementioned four cubic CeO_2 peaks, four extra peaks at 2θ = 29.5.2, 34.4, 49.4 and 58.7° corresponding to cubic ZrO_2 appear with a little bit shift, indicating the successful Zr-doping. However, for sample CeO_2-1T0.25 (Zr:Ce = 1:0.25), only the peaks corresponding to ZrO_2 can be observed, showing that it is predominant by ZrO_2. The crystal size estimated with Scherrer equation (using Sherrer constant of 0.89 and λ of 0.15418 nm) from the (111) XRD peak of CeO_2 are listed in Table 1. The Zr-doping significantly reduces the crystal size of CeO_2 from 18.5 nm to 14.0 nm for Zr:Ce ratio of 1:9, due to the smaller ionic radius of Zr.

Fig. 1b shows the XRD pattens of pure CeO_2, CeO_2-1T9 and their H_2 heat-treated counterparts, *i.e.*, CeO_2_HT and CeO_2-1T9_HT, respectively. The H_2 heat-treated samples show XRD patterns similar to their corresponding ancestors. However, the H_2 heat-treatment process leads to a slight decrease in the crystal size from 18.5 nm for CeO_2 to 18.3 nm for CeO_2_HT, and from 14.0 nm for CeO_2-1T9 to 13.8 nm for CeO_2-1T9_HT, as shown in Table 1.

The N_2 adsorption isotherms at −196 °C and the corresponding pore size distributions of the pure CeO_2 and Zr-doped CeO_2 with various nominal Zr:Ce molar ratios were presented in Fig. 2a and b respectively. All the N_2 adsorption isotherms shown in Fig. 2a exhibit a hysteresis loop at partial pressure (P/P_0) above 0.4, indicating the existence of mesopores in these samples, which is confirmed by the pore size distribution (PSD) shown in Fig. 2b. Meanwhile, all the samples show a very similar bimodal pore size distribution that the majority pores are in the range of 2–5 nm, centred at around 2.8 nm except for CeO_2-1T0.25 which has two peaks entered at 2.8 and 3.8 nm respectively, in addition to a small part of micropores centred at 1.8 nm. The pore sizes of these samples are much smaller than those reported values (*e.g.*, 13.8 nm) [29,37,56]. The BET surface areas of all the samples are summarised in Table 1. The BET surface area of the pure CeO_2 (117 m^2 g^{-1}) is comparable to reported values for CeO_2 prepared by other methods [29,56], but much higher than those prepared by hydrothermal process (74 m^2 g^{-1}) [40] or co-precipitation method (88 m^2 g^{-1}) [37]. The Zr doping up to Zr:Ce = 1:1 can significantly increase the BET surface area from 117 to 176 m^2 g^{-1} (for CeO_2-1T18), but when the Zr:Ce = 1:0.25, the BET surface area is the same as that of pure CeO_2.

Fig. 2c and d show the N_2 adsorption isotherms at −196 °C and the corresponding PSD of pure CeO_2, CeO_2-1 T9 and their H_2 heat-treated counterparts. There is no difference in the N_2 isotherms and PSDs between the as-prepared samples and their H_2 heat-treated counterparts, but the surface area increases after H_2 heat-treatment for both the pure CeO_2 (from 117 to 140 m^2 g^{-1}) and the Zr-doped CeO_2-1T9 (from 133 to 147 m^2 g^{-1}). This increase in surface area could be partially due to the decrease of particle sizes after H_2 heat treatment, which is evidenced by the SEM images shown in Fig. 3. Such surface area enhancement effect is opposite to a report that H_2 heat-treatment at 550 °C causes a decrease in BET surface area of CeO_2 [56]. The reason could be that the preparation process and the H_2 heat-treatment conditions (temperature, heating ramp rate, etc.) for CeO_2 are different between this study and previous report.

The SEM images of CeO_2, CeO_2_HT, CeO_2-1T9, CeO_2-1T9_HT and CeO_2-1T1 are presented in Fig. 3, which reveal that all the samples are made of big lumps and microrods. The microrods of CeO_2 are 12.4——46.3 μm (average 28.6 μm) in length and 3.9——10.3 μm (average 7.9 μm) in width, while that of CeO_2_HT are 10.9——20.3 μm

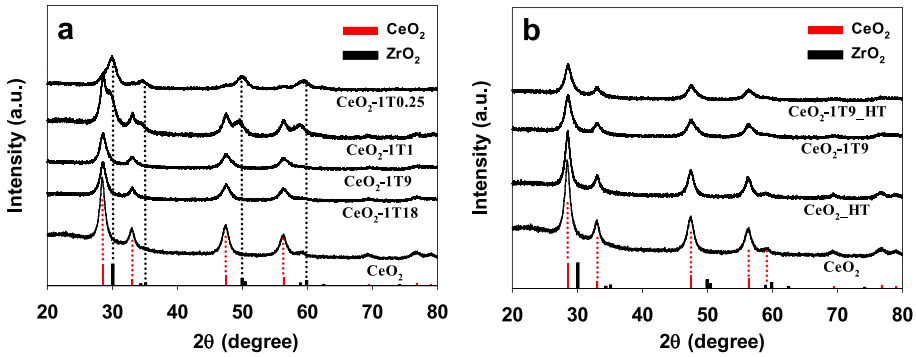

Fig. 1. XRD pattens of (a) pure CeO_2 and Zr-doped CeO_2 with various Zr:Ce molar ratios as well as (b) pure CeO_2, CeO_2-1T9 and their heat-treated counterparts.

Table 1
Properties and catalytic activity of porous CeO_2 and Zr-doped CeO_2.

Sample name	Preparation conditions	Zr:Ce ratio	S_{BET} (m^2 g^{-1})	Crystal size[a] (nm)	CO_2 uptake[b] (mmol g^{-1})	CO_2 uptake[c] (μmol g^{-1})	NH_3 uptake[d] (μmol g^{-1})	Raman I_D/I_{F2g}	XPS Ce^{3+}%	XPS O_v%	DMC formation rate[e] (mmol $g^{-1}h^{-1}$)
CeO_2	400 °C in air	Pure CeO_2	117	18.5	0.68	160.02	**322.27**	0.0086	**23.1**	28.6	**4.05**
CeO_2_HT	400 °C in Air + 400 °C in Ar/H_2 1 h	Pure CeO_2	140	18.3	1.00	129.74	**342.39**	0.0069	**20.4**	25.1	**18.22 ± 0.64**
CeO_2-1T18	400 °C in air	1:18	176	14.9	—	—	—	—	—	—	**2.49**
CeO_2-1T9	400 °C in air	1:9	133	14.0	1.35	159.16	**327.95**	0.0085	**26.3**	31.2	**5.64**
CeO_2-1T9_HT	400 °C in air + 400 °C in Ar/H_2 1 h	1:9	147	13.8	0.83	142.21	**339.78**	0.0090	**32.0**	29.9	**7.19**
CeO_2-1T1	400 °C in air	1:1	138		0.72	28.2	—	—	—	—	**0.99**
CeO_2-1T0.25	400 °C in air	1:0.25	117		0.91	—	—	—	—	—	**0**

[a] Calculated with Scherrer equation from the (1 1 1) XRD peak of CeO_2.
[b] Obtained from CO_2 adsorption analysis with Quantachrome Autosorb-iQ gas analyser at 25 °C.
[c] Obtained from CO_2-TPD (100–300 °C).
[d] Obtained from NH_3-TPD (100–300 °C).
[e] Without applying dehydration agent.

(average 16.6 μm) in length and 3.5——8.7 μm (average 5.8 μm) in width. The microrods of CeO_2-1T9 are 15.7——28.5 μm (average 22.1 μm) in length and 1.4——4.2 μm (average 3.0 μm) in width, while that of CeO_2-1T9_HT are 3.8——13.6 μm in length (average 7.0 μm) and 1.0——2.6 μm (average of 1.5 μm) in width. The microrods of CeO_2-1T1 are 13.3 – 42.9 μm (average 27.8 μm) in length and 3.4——6.1 μm (average 4.9 μm) in width. These results suggest that both the H_2 heat-treatment process and the Zr-doping (except for CeO_2-1T1) will reduce the length and the width of the untreated and undoped CeO_2 microrods.

The pure CeO_2 and CeO_2_HT samples were further investigated by TEM and the images are shown in Fig. 4. Both samples are made of shapeless tiny particles. The (1 1 1) plane with distance of 0.32 nm and the (2 0 0) plane with distance of 0.27 nm can be observed in Fig. 4b for CeO_2, but only the (1 1 1) plane with distance of 0.32 nm can be observed in Fig. 4d for CeO_2_HT, indicating that the H_2 heat-treatment process promote the exposure of the (1 1 1) plane.

3.2. Acid-base properties

The surface acid-base properties of pure CeO_2, CeO_2-1T9, and their corresponding H_2 heat-treated counterparts were measured by NH_3-TPD and CO_2-TPD, and the obtained profiles are shown in Fig. 5. The NH_3-TPD profiles in Fig. 5a show a major broad desorption peak in the temperature range of 100——300 °C for all the samples, suggesting the presence of weak acidity. In addition, a weak extra peak appears at 311 °C for CeO_2, which disappears after H_2 heat-treatment. The centre of the major NH_3 desorption peak shifts from 185 °C for CeO_2 to 179 °C for CeO_2_HT, but it remains at 196 °C for the Zr-doped samples CeO_2-1T9 and CeO_2-1T9_HT.

The CO_2-TPD profiles in Fig. 5b also show a major broad desorption peak in the temperature range of 100——300 °C for all the samples, suggesting the presence of weak basicity. In addition, a weak extra peak appears at 323 °C for CeO_2, which disappears after H_2 heat-treatment. The centre of the major CO_2 desorption peak shifts from 173 °C for CeO_2 to 159 °C for CeO_2_HT, and from 178 °C for CeO_2-1T9 to 165 °C CeO_2-1T9_HT. This shift could contribute to the catalytic activity toward CO_2 conversion into DMC as discussed later.

3.3. Defects, Ce^{3+} concentrations, and O_V concentrations

Raman spectroscopy measurement was carried out to study the defects of selected samples. Fig. 6 shows the Raman spectra (532 nm laser) of pure CeO_2, CeO_2-1T9 and their H_2 heat-treated counterparts. All the samples show peaks at 260.8, 462.8, and 601.6 cm^{-1}, corresponding to the second-order 2TA peak, the first-order F_{2g} peak, and the defect-induced (D) peak respectively [62,63]. As shown in Fig. 6a, there is no obvious difference in the F_{2g} peak intensity between CeO_2 and CeO_2-1T9, suggesting that the Zr-doping does not significantly change the structure of CeO_2. This is in agreement with the above XRD results. Fig. 6a also reveals that there is no obvious difference in the F_{2g} peak between CeO_2-1T9 and CeO_2-1T9_HT, but there is a huge increase in the F_{2g} peak intensity of CeO_2_HT. This intensity increase could be due to more favourable surface termination of CeO_2 induced by the H_2 heat-treatment process, which is supported by the TEM image (shown in Fig. 4) that the surface termination is dominated by the (1 1 1) plane for CeO_2_HT, while both the (1 1 1) and the (2 0 0) planes are observable for

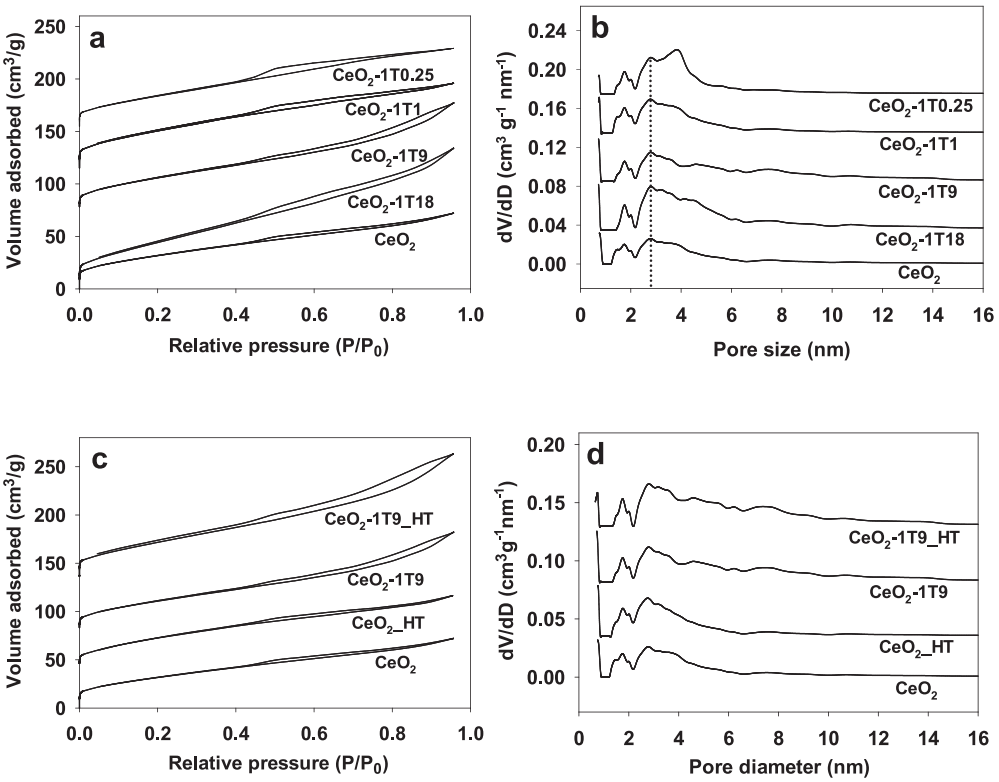

Fig. 2. (a) N_2 adsorption isotherms at −196 °C and (b) corresponding pore size distributions (PSD) of pure CeO_2 and Zr-doped CeO_2 with various Zr:Ce molar ratios. (c) N_2 adsorption isotherms at −196 °C and (d) corresponding pore size distributions (PSD) of pure CeO_2, CeO_2-1T9 and their H_2 heat-treated counterparts. The isotherms in (a) were offset by 70 for CeO_2-1T9, 115 for CeO_2-1T1, and 155 for CeO_2-1T0.25. The PSD curves in (b) were offset by 0.035 for CeO_2-1T18, 0.08 for CeO_2-1T9, 0.135 for CeO_2-1T1, and 0.175 for CeO_2-1T0.25. The isotherms in (c) were offset by 35 for CeO_2_HT, 75 for CeO_2-1T9, and 135 for CeO_2-1T9_HT. The PSD curves in (d) were offset by 0.035 for CeO_2_HT, 0.082 for CeO_2-1T9, and 0.13 for CeO_2-1T9_HT.

CeO_2. Regarding the defect-induced peak (D peak) at 601.6 cm^{-1}, Fig. 6b shows that the D peak intensity of CeO_2_HT and CeO_2-1T9_HT significantly increases compared with that of CeO_2 and CeO_2-1T9, respectively. In addition, the D peak intensity of CeO_2-1T9 slightly increases compared to that of CeO_2. The intensity ratio of the D peak to the F_{2g} peak (I_D/I_{F2g}) has been widely used to indicate the amount of defects of CeO_2-based catalysts [29,40,64]. Although the peak intensity of both the F_{2g} peak and the D peak of CeO_2_HT increases, the extent in peak intensity increase of these two peaks is different. As shown in Table 1, CeO_2_HT exhibits lower I_D/I_{F2g} value of 0.0069 compared to that of CeO_2 (0.0086), while CeO_2-1T9_HT shows higher I_D/I_{F2g} value of 0.0090 compared to that of CeO_2-1T9 (0.0085), indicating that the H_2 heat-treatment reduces the amount of defects for CeO_2 but promotes the amount of defects for Zr-doped CeO_2.

The XPS spectra of selected samples are shown in Fig. 7. For the Ce 3d spectra, 8 peaks of μ_0 (~885.6 eV), μ_1 (~881.4 eV), μ_0' (~903.5 eV), μ_1' (~899.2 eV), ν_0 (~882.6 eV), ν_1 (~888.9 eV), ν_2 (~898.3 eV), ν_0' (~900.9 eV), ν_1' (~907.5 eV), ν_2' (~916.7 eV) can be deconvoluted, corresponding to the spin–orbit splitting of Ce $3d_{5/2}$ (μ_0, μ_1, ν_0, ν_1, ν_2) and Ce $3d_{3/2}$ (μ_0', μ_1', ν_0', ν_1', ν_2'), respectively [64–66]. The concentration of Ce^{3+} (Ce^{3+} %) is calculated from the ratio of peak areas of Ce^{3+} (μ_0, μ_1, μ_0', μ_1') to peak areas of Ce^{3+} and Ce^{4+} (ν_0, ν_1, ν_2, ν_0', ν_1', ν_2') based on the equation below:

$$Ce^{3+}\% = \frac{Peakareaof\,Ce^{3+}}{Peakareaof\,(Ce^{3+}+Ce^{4+})} \times 100$$

The calculated Ce^{3+}% are listed in Table 1, which are 23.1 (CeO_2), 20.4 (CeO_2_HT), 26.3 (CeO_2-1T9) and 27.1 (CeO_2-1T9_HT). The results reveal that the addition of Zr to CeO_2 can significantly increase the surface Ce^{3+}%, which is in good agreement with literature report [40]. In addition, the H_2 heat-treatment of Zr-doped CeO_2 (CeO_2-1T9) results in an increase in surface Ce^{3+}% of CeO_2-1T9_HT, accordingly an increase in Ce^{3+}-associated defects, which is consistent with the above Raman results that more defects are found for the H_2 heat-treated sample (CeO_2-1T9_HT) compared to its counterpart, CeO_2-1T9. This increase in surface Ce^{3+}% effect due to H_2 heat-treatment is also in good agreement with literature report [56]. However, in the case of pure CeO_2, H_2 heat-treatment leads to reduced surface Ce^{3+}% of the resulting CeO_2_HT, consequently less amount of Ce^{3+}-associated defects in sample CeO_2_HT. This is consistent with the above Raman results that H_2 heat-treatment of pure CeO_2 leads to less amount of defects, although it is opposite to Zhang *et al.*'s report that H_2 heat-treatment promotes the conversion of Ce^{4+} to Ce^{3+} [56]. This contrary could be due to the following reasons: (i) the H_2 heat-treatment conditions are different between these two studies; (ii) the strategies used for the CeO_2 preparation in these two studies are different, resulting in CeO_2 with different properties and consequently leading to different responses to H_2 heat-treatment.

The H_2-TPR results are shown in Fig. S4, the peak between 300 and 600 °C of CeO_2 could be due to the reduction of surface oxygen species such as oxygen attached to Ce^{4+} [67] and surface hydroxyl groups [68], with a H_2 consumption of 1.94 mmol g^{-1}. However, the peak shifts to higher temperature at 400–600 °C for CeO_2_HT with a H_2 consumption of 0.159 mmol g^{-1}. Although the H_2 consumption of CeO_2 is much higher than that of CeO_2_HT, it does not necessarily mean that CeO_2 has higher amount of Ce^{3+} than CeO_2_HT, as the H_2 consumption of CeO_2 could be due to the reduction of Ce^{4+} to Ce^{3+} and the reaction of hydroxyl groups. However, based on these results, it can be concluded that the H_2 heat-treatment at 400 °C can significantly reduce surface oxygen species of CeO_2, which could lead to less defects.

For O 1 s XPS spectra, 3 peaks at ~529.4, ~531.5, and ~533.5 eV corresponding to the lattice oxygen (O_L), oxygen vacancy (O_V), and

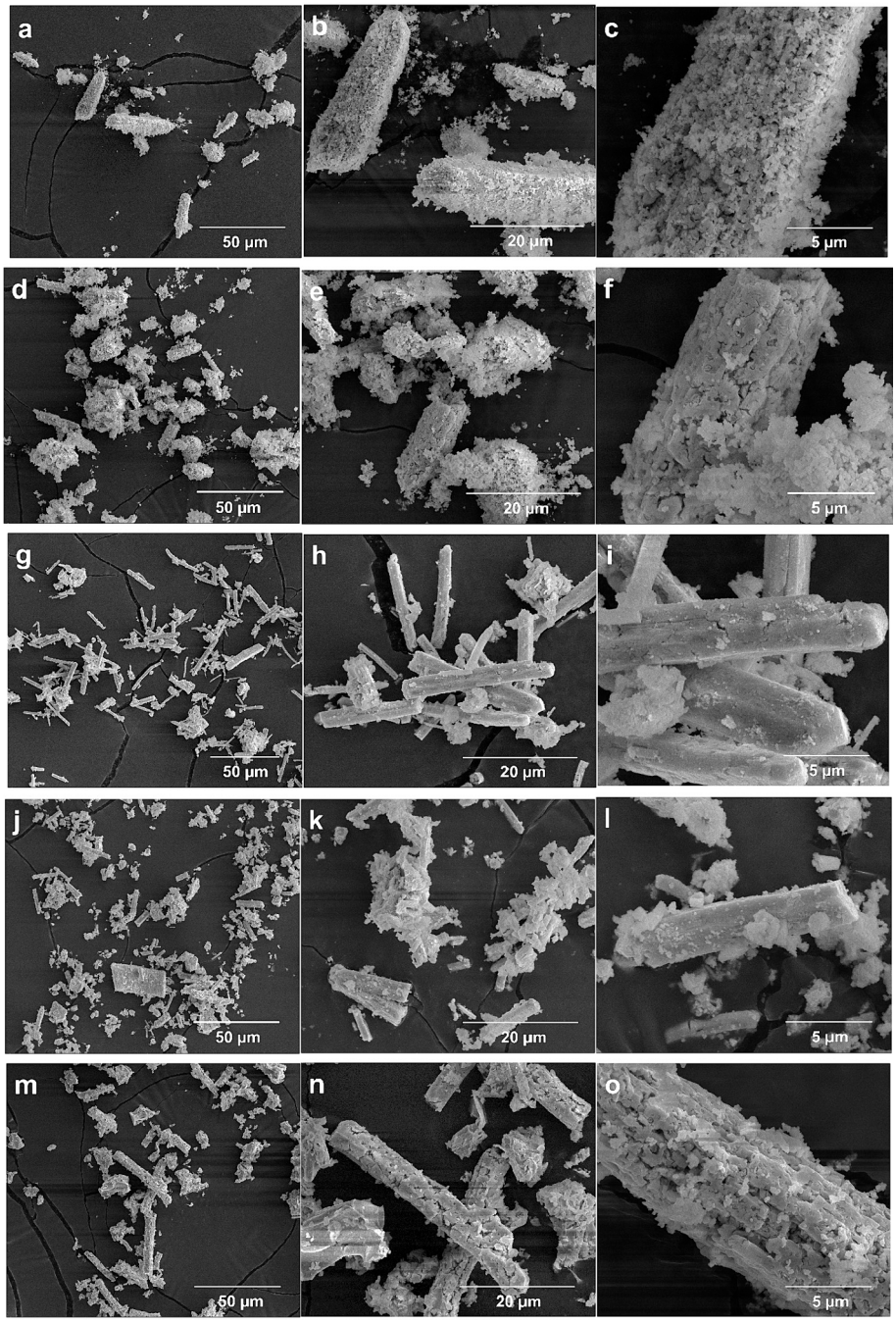

Fig. 3. SEM images of (a-c) CeO_2, (d-e) CeO_2_HT, (f-h) CeO_2-1T9, (i-l) CeO_2-1T9_HT, and (m-o) CeO_2-1T1.

chemisorbed oxygen (O_C), respectively can be deconvoluted [29,40]. The O_V peak shifts from 531.2 eV for CeO_2 to 531.5 eV for CeO_2_HT, and from 531.5 eV for CeO_2-1T9 to 531.7 eV for CeO_2-1T9_HT, showing an increase in binding energy resulted from H_2 heat- treatment for both the pure CeO_2 and the Zr-doped CeO_2. The concentration of surface oxygen vacancies is calculated from the ratio of peak areas of O_V to peak areas of O_L, O_V and O_C based on the equation below:

$$O_V\% = \frac{Peakareaof\,O_V}{Peakareaof\,(O_L + O_V + O_C)} \times 100$$

The calculated O_V% are listed in Table 1, revealing an increase in O_V% resulted from Zr doping, which is consistent to literature report [40,69]. However, the O_V% reduces after H_2 heat- treatment for both the pure CeO_2 and the Zr-doped CeO_2. The decrease of O_V% agrees well with the decrease of Ce^{3+}% resulted from H_2 heat-treatment for pure CeO_2, as O_V is associated with Ce^{3+}. The increase in Ce^{3+}% accompanied with the decrease of O_V % after H_2 heat- treatment for the Zr-doped CeO_2 could be due to the effect of Zr-doping (leading to Ce^{3+}% increase).

3.4. Catalytic activity

The catalytic activity of the samples towards the direct conversion of CO_2 into DMC was evaluated by the DMC formation rate, which is listed in Table 1. The CeO_2 sample exhibits a DMC formation rate of 4.05 mmol $g^{-1}h^{-1}$. Upon Zr-doping, the DMC formation rate slightly increases to 5.64 mmol $g^{-1}h^{-1}$ for CeO_2-1T9 (with a nominal Zr:Ce ratio of 1:9), but it decreases for other Zr-doped samples with various nominal Zr:Ce ratios, indicating that the best Zr:Ce ratio is 1:9. In addition, the H_2

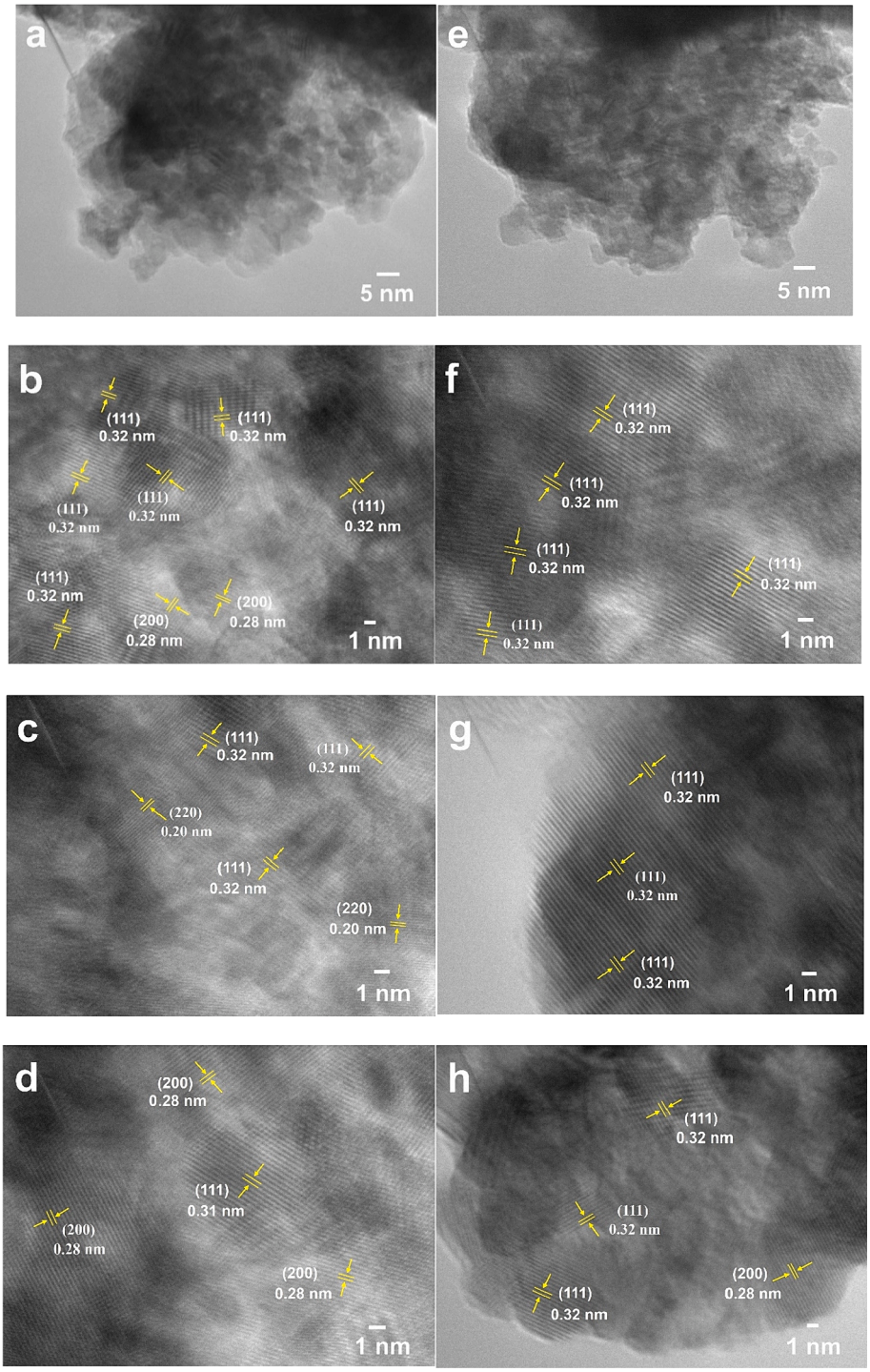

Fig. 4. TEM images of (a-d) CeO_2 and (e-h) CeO_2_HT.

heat-treatment process can enhance the DMC formation rate from 5.64 mmol $g^{-1}h^{-1}$ of CeO_2-1T9 to 7.19 mmol $g^{-1}h^{-1}$ of CeO_2-1T9_HT. Interestingly, the H_2 heat-treatment of CeO_2 can remarkably improve the DMC formation rate to 18.22 ± 0.64 mmol $g^{-1}h^{-1}$ (CeO_2_HT), which is among the highest DMC formation rate for pure CeO_2 catalysts at 140 °C. These results demonstrate that Zr-doping with the appropriate Zr:Ce ratio can increase the DMC formation rate of the resulting Zr-doped CeO_2, in agreement with reports [40]. In addition, the H_2 heat-treatment can significantly enhance the DMC formation rate of pure CeO_2 catalyst, and mildly improve the DMC formation rate of the Zr-doped CeO_2 catalyst in this study. A comparison of the preparation method, DMC formation rate of CeO_2 catalysts and metal doped CeO_2 catalysts between some reported work and this study is summarised in Table S1, indicating that this research provides a low temperature synthesis strategy for CeO_2 catalyst with high DMC formation rate.

Based on Table 1, the ability to physically adsorb CO_2 at room temperature (25 °C) of the samples has no effect on the DMC formation rate. Fig. 8 reveals the effect of the BET surface area, base property, acid property, O_V%, Ce^{3+}%, and the Raman peak intensity ratio of I_D/I_{F2g} on the DMC formation rate. In all cases, the DMC formation rate of the H_2 heat-treated sample CeO_2_HT is exceptionally high. Excluding this best performed catalyst (CeO_2_HT), for the rest catalysts in this study, the

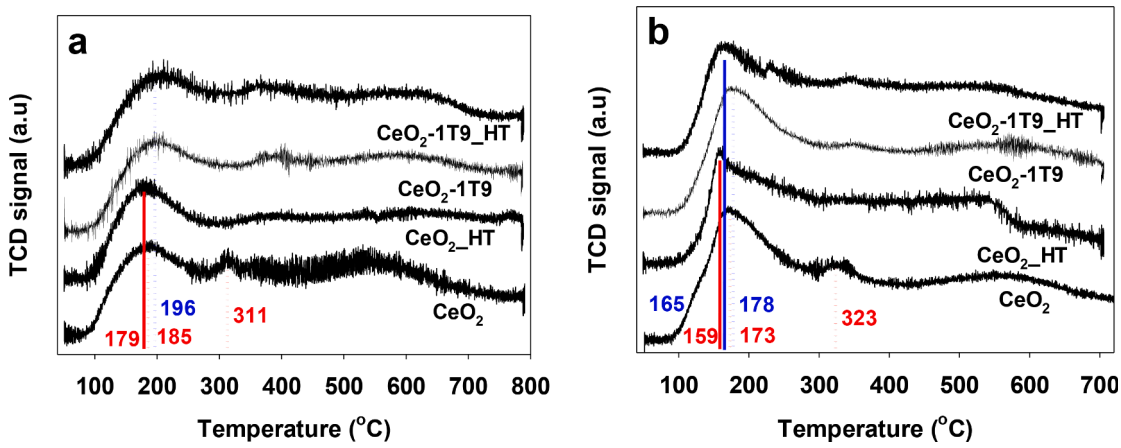

Fig. 5. (a) NH_3-TPD and (b) CO_2-TPD profiles of pure CeO_2, CeO_2-1T9, and their H_2 heat- treated counterparts.

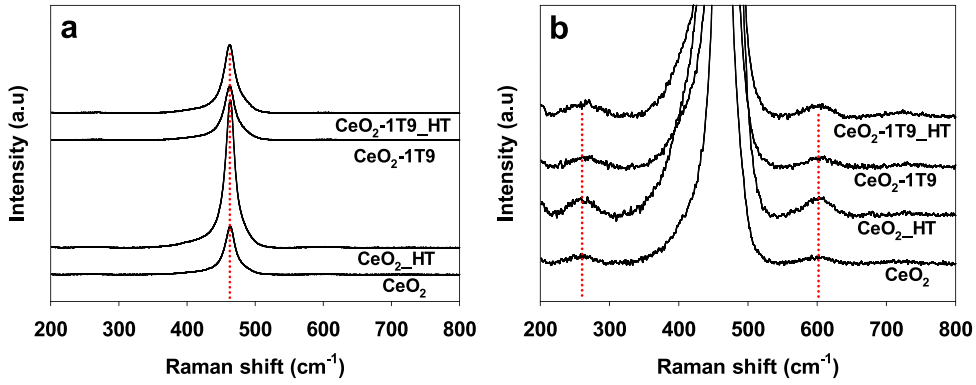

Fig. 6. (a) Full scale and (b) zoomed in Raman shifts of pure CeO_2, CeO_2-1T9 and their H_2 heat-treated counterparts.

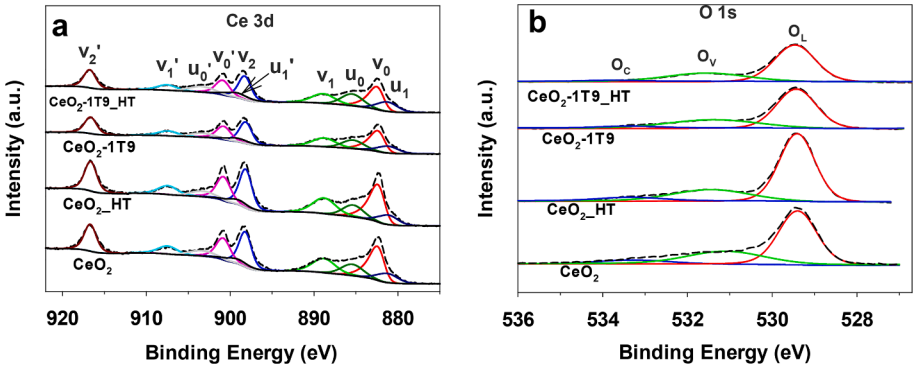

Fig. 7. XPS spectra of (a) Ce 3d and (b) O 1 s of pure CeO_2, CeO_2-1 T9, and their H_2-heat treated counterparts.

DMC formation rate has a positive link to the BET surface area, acid property (NH_3-TPD), O_V%, Ce^{3+}%, and the Raman peak intensity ratio of I_D/I_{F2g} of the catalyst, demonstrating that these properties facilitate the DMC formation, which agrees well with reports [12,29,32,35–37,40,70]. Nevertheless, it seems there is no link (or a slightly negative link) between the DMC yield and the base property (CO_2-TPD). The explanation could be that the effect of the base property is not as influential as other factors in this study. Based on the above discussion, it can be suggested that the formation of DMC is multi-factor controlled [45] and there could be an optimised combination of these factors for the best catalytic activity. An attempt explanation for the exceptional DMC formation rate enhanced by the H_2 heat-treatment of the CeO_2 catalyst is as follows.

(i) Although oxygen vacancy is thought to improve the DMC formation, it is also suggested that areas with high oxygen vacancies where some of the carbonates can be trapped will activate the internal bonds in undesired manners, which would make the enrichment of more oxygen vacancies less efficient in DMC formation [71]. Therefore, in this study, the H_2 heat-treatment process reduces the defects (O_V% and Ce^{3+}%) as supported by the Raman and XPS results, which could result in a balanced crystallinity and defects to achieve high DMC formation rate.

(ii) It is well known that surface acid-base properties can facilitate the formation of DMC [33,35,36,41]. In this study, the H_2 heat-treatment leads to more acid sites, and a shift of acid-base activity to lower temperature as proved by NH_3-TPD and CO_2-TPD, which may significantly improve the DMC formation rate.

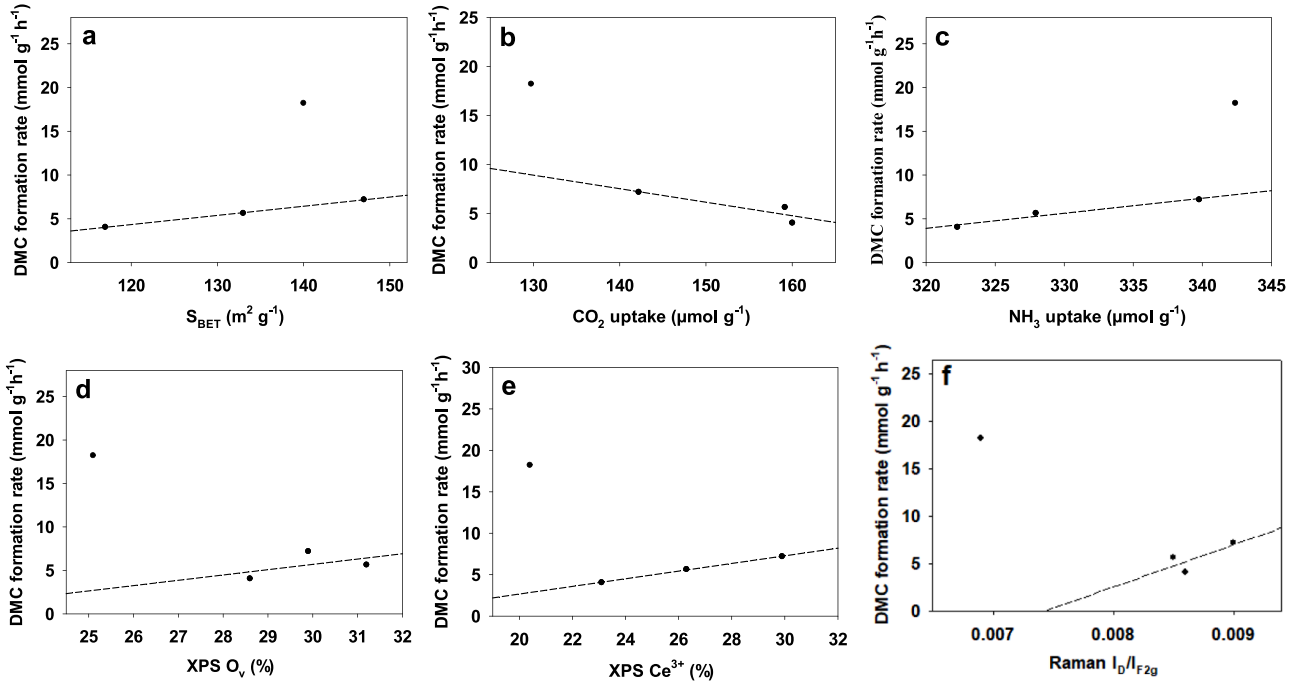

Fig. 8. Effect of various parameters on DMC formation rate: (a) Surface area S_{BET}, (b) Base property, (c) Acid property, (d) XPS O_V%, (e) XPS Ce^{3+}%, (f). Raman peak intensity ratio of I_D/I_{F2g}.

(iii) It is reported that the (1 1 1) surface is the most stable plane against the formation of surface oxygen vacancies [72,73], and theoretical study has shown that (1 1 1) is the least active surface [74]. However, it is suggested that the active site of the reaction is on a stable crystal surface such as (1 1 1) of CeO_2 [12]. Moreover, it has been demonstrated that CeO_2 with (1 1 1) surface was more active than CeO_2 with (1 0 0) and (1 1 0) for CO oxidation [75]. In addition, Senanayake et al. reported that the surface of reduced CeO_2 with (1 1 1) plane is more active than that of the oxidised CeO_2 with (1 1 1) plane [76]. In this study, the H_2 heat-treatment leads to the promotion of the exposure of the (1 1 1) plane supported by the TEM images, which could play a major role in the enhancement of the DMC formation rate.

The CeO_2_HT sample with the exceptionally high DMC formation rate was further studied by in-situ diffuse reflectance infrared Fourier transform spectroscopy (DRIFTS) [29] measurement to investigate the DMC formation mechanism. Fig. 9 shows the in-situ DRIFTS spectra of CeO_2_HT with pre-adsorbed methanol followed by purging CO_2 at 140 °C. Bands at 1574, 1290 and 1016 cm^{-1} are assigned to bidentate carbonate. Bands at 1051 and 1033 cm^{-1} are assigned to bridged methoxy and bands at 1100 cm^{-1} are on-top methoxy species. Bands at 1590, 1364 and 1349 cm^{-1} are monomethyl carbonate and bands at 1443, 1363 and 1016 cm^{-1} are monodentate carbonate [29,77]. Bidentate carbonate is originated from CO_2 adsorption and the methoxy species are from methanol adsorption. As shown in Fig. 9, the decrease of the on-top methoxy species is accompanied by the appearance of monomethyl carbonate, suggesting that the on-top methoxy reacts with bidentate carbonate to form monomethyl carbonate, which further reacts with another on-top methoxy species to generate DMC [29,78]. The proposed DMC formation steps are presented in Scheme 1.

After the reaction testing, CeO_2_HT catalyst was recycled by centrifugation followed by H_2O washing and air calcination at 400 °C. The DMC formation rate of recycled CeO_2_HT is 16.9 mmol $g^{-1}h^{-1}$, which is slightly lower than the fresh CeO_2_HT. The declined activity could be due to the blockage of surface active site by the reaction residue [29]. The XRD and Raman of CeO_2_HT catalyst before and after the catalytic use are shown in Fig. S5. There is no significant differences in XRD of CeO_2_HT before and after the catalytic use. Furthermore, the defect-

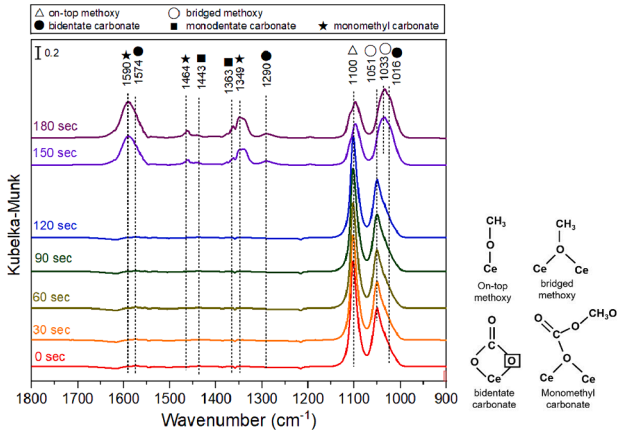

Fig. 9. In-situ DRIFTS spectra of CeO_2_HT with pre-adsorbed methanol followed by purging CO_2 at 140 °C.

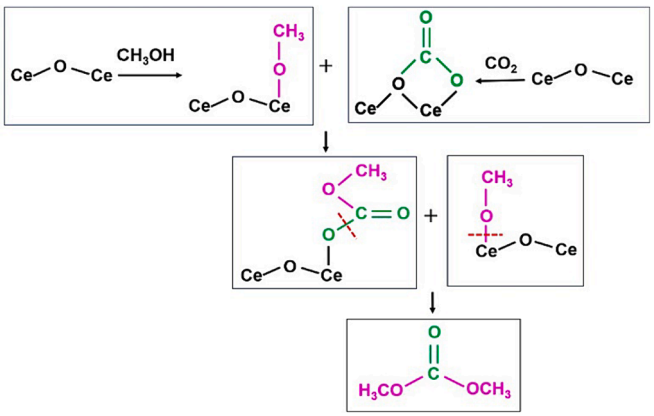

Scheme 1. Proposed mechanism of DMC formation from CO_2 and methanol over H_2 heat-treated CeO_2 (CeO_2_HT).

induced Raman peaks at *ca.* 600 cm^{-1} for CeO_2_HT before and after the catalytic use are identical, suggesting the defect level is almost unchanged. The reduced intensity of Raman peak at *ca.* 260 cm^{-1} observed on recycled CeO_2_HT suggests a decrease in surface area after the catalytic use [58].

4. Conclusions

In this study, porous CeO_2 and Zr-doped CeO_2 catalysts with high surface area have been prepared via low temperature synthesis strategy and evaluated for the direct conversion of CO_2 and methanol into DMC. Results show that Zr-doping can slightly increase the DMC formation rate of the resulting Zr-doped catalyst with the appropriate Zr:Ce nominal ratio of (1:9), and a further H_2 heat-treatment step of the catalysts can remarkably enhance the DMC formation rate of the resulting pure CeO_2 catalyst and slightly increase the DMC formation rate of the resulting Zr-doped CeO_2 catalyst. An exceptionally high DMC formation rate of 18.22 ± 0.64 mmol $g^{-1}h^{-1}$has been achieved for the H_2 heat-treated CeO_2, which is the among the highest for pure CeO_2 catalysts at 140 °C ever reported. The huge improvement in DMC formation rate could be mainly due to a balanced crystallinity and defects of the CeO_2, a shift of acid and base activity to lower temperature, and the (1 1 1) plane only exposure of the catalyst resulted from the H_2 heat-treatment process. Excluding the H_2 heat-treated CeO_2 catalyst that exhibits the highest DMC formation rate, there is a positive link between the DMC yield and the BET surface area, acid property (NH_3-TPD), O_V%, Ce^{3+}%, and the Raman peak intensity ratio of I_D/I_{F2g} of the rest catalysts. This study provides a low temperature preparation method for CeO_2 catalyst with extremely high catalytic activity towards the direct conversion of CO_2 and methanol into DMC, which could be applicable to other reactions (*e.g.*, the synthesis of diethyl carbonate) too.

Author contribution

The manuscript was written through the contributions of all authors. All authors have given approval to the final version of the manuscript.

CRediT authorship contribution statement

Zhuxian Yang: Writing – original draft, Methodology, Investigation, Data curation. **Monica Mengdie Lin:** Writing – review & editing, Validation, Methodology, Data curation. **Xinhuan Lu:** Validation, Methodology, Data curation. **Justin Tay Zheng:** Validation, Methodology, Investigation, Data curation. **Wen-Yueh Yu:** Writing – review & editing, Supervision. **Yanqiu Zhu:** Writing – review & editing, Supervision. **Hong Chang:** Investigation, Data curation. **Yongde Xia:** Writing – review & editing, Validation, Supervision, Methodology, Conceptualization.

Declaration of competing interest

The authors declare that they have no known competing financial interests or personal relationships that could have appeared to influence the work reported in this paper.

Data availability

No data was used for the research described in the article.

Acknowledgements

This work was supported by the Leverhulme Trust (RPG-2018–320) and the Royal Society (IEC\NSFC\201121). WYY is grateful for the financial support from the National Science and Technology Council (NSTC), Taiwan (110-2221-E-002-012-MY3, and 112-2221-E-002-041-MY3).

Appendix A. Supplementary data

Supplementary data to this article can be found online at https://doi.org/10.1016/j.cej.2024.150339.

References

[1] G. Fiorani, A. Perosa, M. Selva, Dimethyl carbonate: a versatile reagent for a sustainable valorization of renewables, Green Chem. 20 (2018) 288–322, https://doi.org/10.1039/c7gc02118f.
[2] Y. Ono, Catalysis in the production and reactions of dimethyl carbonate, an environmentally benign building block, Appl. Catal. A 155 (1997) 133–166, https://doi.org/10.1016/s0926-860x(96)00402-4.
[3] M.A. Pacheco, C.L. Marshall, Review of dimethyl carbonate (DMC) manufacture and its characteristics as a fuel additive, Energy Fuels 11 (1997) 2–29, https://doi.org/10.1021/ef9600974.
[4] P. Kumar, V.C. Srivastava, U.L. Stangar, B. Music, I.M. Mishra, Y.Z. Meng, Recent progress in dimethyl carbonate synthesis using different feedstock and techniques in the presence of heterogeneous catalysts, Catal. Rev. 63 (2021) 363–421, https://doi.org/10.1080/01614940.2019.1696609.
[5] H. Babad, A.G. Zeiler, Chemistry of phosgene, Chem. Rev. 73 (1973) 75–91, https://doi.org/10.1021/cr60281a005.
[6] J.Q. Wang, J. Sun, W.G. Cheng, C.Y. Shi, K. Dong, X.P. Zhang, S.J. Zhang, Synthesis of dimethyl carbonate catalyzed by carboxylic functionalized imidazolium salt via transesterification reaction,, Catal. Sci. Technol. 2 (2012) 600–605, https://doi.org/10.1039/c1cy00342a.
[7] J. Xu, K.Z. Long, T. Chen, B. Xue, Y.X. Li, Y. Cao, Mesostructured graphitic carbon nitride as a new base catalyst for the efficient synthesis of dimethyl carbonate by transesterification,, Catal. Sci. Technol. 3 (2013) 3192–3199, https://doi.org/10.1039/c3cy00517h.
[8] U. Romano, R. Tesei, M.M. Mauri, P. Rebora, Synthesis of dimethyl carbonate from methanol, carbon-monoxide, and oxygen catalyzed by copper-compounds, Ind. Eng. Chem. Prod. Res. Dev. 19 (1980) 396–403, https://doi.org/10.1021/i360075a021.
[9] M.J. Schneider, M. Haumann, M. Stricker, J. Sundermeyer, P. Wasserscheid, Gas-phase oxycarbonylation of methanol for the synthesis of dimethyl carbonate using copper-based supported ionic liquid phase (SILP) catalysts, J. Catal. 309 (2014) 71–78, https://doi.org/10.1016/j.jcat.2013.08.029.
[10] H.Z. Tan, Z.Q. Wang, Z.N. Xu, J. Sun, Z.N. Chen, Q.S. Chen, Y.M. Chen, G.C. Guo, Active PD(II) complexes: enhancing catalytic activity by ligand effect for carbonylation of methyl nitrite to dimethyl carbonate, Catal. Sci. Technol. 7 (2017) 3785–3790, https://doi.org/10.1039/c7cy01305a.
[11] D.C. Shi, S. Heyte, M. Capron, S. Paul, Catalytic processes for the direct synthesis of dimethyl carbonate from CO_2 and methanol: a review, Green Chem. 24 (2022) 1067–1089, https://doi.org/10.1039/d1gc04093f.
[12] Y. Yoshida, Y. Arai, S. Kado, K. Kunimori, K. Tomishige, Direct synthesis of organic carbonates from the reaction of CO_2 with methanol and ethanol over CeO_2 catalysts, Catal. Today 115 (2006) 95–101, https://doi.org/10.1016/j.cattod.2006.02.027.
[13] L.G. Wang, Y. Wang, S.M. Liu, L.J. Lu, X.Y. Ma, Y.Q. Deng, Efficient synthesis of dimethyl carbonate via transesterification of ethylene carbonate with methanol over binary zinc-yttrium oxides, Catal. Commun. 16 (2011) 45–49, https://doi.org/10.1016/j.catcom.2011.09.004.
[14] Z.Q. Hou, L.G. Luo, K. Liu, C.Z. Liu, Y.Y. Wang, L.Y. Dai, High-yield synthesis of dimethyl carbonate from the direct alcoholysis of urea in supercritical methanol, Chem. Eng. J. 236 (2014) 415–418, https://doi.org/10.1016/j.cej.2013.09.024.
[15] K. Tomishige, T. Sakaihori, Y. Ikeda, K. Fujimoto, A novel method of direct synthesis of dimethyl carbonate from methanol and carbon dioxide catalyzed by zirconia, Catal. Lett. 58 (1999) 225–229, https://doi.org/10.1023/a:1019098405444.
[16] B. Peng, H.R. Dou, H. Shi, E.E. Ember, J.A. Lercher, Overcoming thermodynamic limitations in dimethyl carbonate synthesis from methanol and CO_2, Catal. Lett. 148 (2018) 1914–1919, https://doi.org/10.1007/s10562-018-2402-8.
[17] K. Tomishige, K. Kunimori, Catalytic and direct synthesis of dimethyl carbonate starting from carbon dioxide using CeO_2-ZrO_2 solid solution heterogeneous catalyst: effect of H_2O removal from the reaction system, Appl. Catal. A 237 (2002) 103–109, https://doi.org/10.1016/s0926-860x(02)00322-8.
[18] J.C. Choi, L.N. He, H. Yasuda, T. Sakakura, Selective and high yield synthesis of dimethyl carbonate directly from carbon dioxide and methanol, Green Chem. 4 (2002) 230–234, https://doi.org/10.1039/b200623p.
[19] Z.F. Zhang, Z.W. Liu, J.A. Lu, Z.T. Lie, Synthesis of dimethyl carbonate from carbon dioxide and methanol over $Ce_xZr_{1-x}O_2$ and EMIM Br/$Ce_{0.5}Zr_{0.5}O_2$, Ind. Eng. Chem. Res., 50 (2011) 1981-1988. DOI: 10.1021/ie102017j.
[20] N. Wang, Y. Liu, A. Huang, J. Caro, Hydrophilic SOD and LTA membranes for membrane-supported methanol, dimethylether and dimethylcarbonate synthesis, Microporous Mesoporous Mater. 207 (2015) 33–38, https://doi.org/10.1016/j.micromeso.2014.12.028.
[21] S.N. Fang, K. Fujimoto, Direct synthesis of dimethyl carbonate from carbon dioxide and methanol catalyzed by base, Appl. Catal. A 142 (1996) L1–L3, https://doi.org/10.1016/0926-860x(96)00081-6.
[22] T. Sakakura, J.C. Choi, Y. Saito, T. Sako, Synthesis of dimethyl carbonate from carbon dioxide: catalysis and mechanism, Polyhedron 19 (2000) 573–576, https://doi.org/10.1016/s0277-5387(99)00411-8.

[23] J. Kizlink, I. Pastucha, Preparation of dimethl carbonate from methanol and carbon dioxide in the presence of sn (IV) and ti (IV) alkoxides and metal acetates, collect. czechoslov, Chem. Commun. 60 (1995) 687–692, https://doi.org/10.1135/cccc19950687.

[24] X.L. Wu, M. Xiao, Y.Z. Meng, Y.X. Lu, Direct synthesis of dimethyl carbonate on H_3PO_4 modified V_2O_5, J. Mol. Catal. A Chem. 238 (2005) 158–162, https://doi.org/10.1016/j.molcata.2005.05.018.

[25] W. Sun, L. Zheng, Y.Q. Wang, D.D. Li, Z.R. Liu, L. Wu, T. Fang, J.Q. Wu, Study of thermodynamics and experiment on direct synthesis of dimethyl carbonate from carbon dioxide and methanol over yttrium oxide, Ind. Eng. Chem. Res. 59 (2020) 4281–4290, https://doi.org/10.1021/acs.iecr.9b06092.

[26] K.T. Jung, A.T. Bell, An in situ infrared study of dimethyl carbonate synthesis from carbon dioxide and methanol over zirconia, J. Catal. 204 (2001) 339–347, https://doi.org/10.1006/jcat.2001.3411.

[27] C.J. Jiang, Y.H. Guo, C.G. Wang, C.W. Hu, Y. Wu, E.B. Wang, Synthesis of dimethyl carbonate from methanol and carbon dioxide in the presence of polyoxometalates under mild conditions, App. Catal. A 256 (2003) 203–212, https://doi.org/10.1016/s0926-860x(03)00400-9.

[28] Q.X. Zheng, R. Nishimura, Y. Sato, H. Inomata, M. Ota, M. Watanabe, S. Camy, Dimethyl carbonate (DMC) synthesis from methanol and carbon dioxide in the presence of ZrO_2 solid solutions and yield improvement by applying a natural convection circulation system, Chem. Eng. J. 429 (2022) 132378, https://doi.org/10.1016/j.cej.2021.132378.

[29] W.F. Kuan, W.Y. Yu, F.Y. Tu, C.H. Chung, Y.C. Chang, M.M. Lin, T.H. Yu, L.J. Chen, Facile reflux preparation of defective mesoporous ceria nanorod with superior catalytic activity for direct carbon dioxide conversion into dimethyl carbonate, Chem. Eng. J. 430 (2022) 132941, https://doi.org/10.1016/j.cej.2021.132941.

[30] H.J. Lee, W. Joe, I.K. Song, Direct synthesis of dimethyl carbonate from methanol and carbon dioxide over transition metal oxide/$Ce_{0.6}Zr_{0.4}O_2$ catalysts: effect of acidity and basicity of the catalysts, Korean J. Chem. Eng. 29 (2012) 317–322, https://doi.org/10.1007/s11814-011-0185-3.

[31] K. Tomishige, Y. Gu, T. Chang, M. Tamura, Y. Nakagawa, Catalytic function of CeO_2 in non-reductive conversion of CO_2 with alcohols, Mater. Today Sustain. 9 (2020) 100035, https://doi.org/10.1016/j.mtsust.2020.100035.

[32] E. Leino, N. Kumar, P. Maki-Arvela, A. Aho, K. Kordas, A.R. Leino, A. Shchukarev, D.Y. Murzin, J.P. Mikkola, Influence of the synthesis parameters on the physico-chemical and catalytic properties of cerium oxide for application in the synthesis of diethyl carbonate, Mater. Chem. Phys. 143 (2013) 65–75, https://doi.org/10.1016/j.matchemphys.2013.08.012.

[33] B. Liu, C.M. Li, G.Q. Zhang, L.F. Yan, Z. Li, Direct synthesis of dimethyl carbonate from CO_2 and methanol over CaO-CeO_2 catalysts: the role of acid-base properties and surface oxygen vacancies, New J. Chem. 41 (2017) 12231–12240, https://doi.org/10.1039/c7nj02606d.

[34] K.W. La, J.C. Jung, H. Kim, S.H. Baeck, I.K. Song, Effect of acid-base properties of $H_3PW_{12}O_{40}/Ce_xTi_{1-x}O_2$ catalysts on the direct synthesis of dimethyl carbonate from methanol and carbon dioxide: a TPD study of $H_3PW_{12}O_{40}/Ce_xTi_{1-x}O_2$ catalysts, J. Mol. Catal. A 269 (2007) 41–45, https://doi.org/10.1016/j.molcata.2007.01.006.

[35] H.J. Lee, S. Park, I.K. Song, J.C. Jung, Direct synthesis of dimethyl carbonate from methanol and carbon dioxide over $Ga_2O_3/Ce_{0.6}Zr_{0.4}O_2$ catalysts: effect of acidity and basicity of the catalysts, Catal. Lett. 141 (2011) 531–537, https://doi.org/10.1007/s10562-010-0544-4.

[36] H.J. Lee, W. Joe, J.C. Jung, I.K. Song, Direct synthesis of dimethyl carbonate from methanol and carbon dioxide over Ga_2O_3-CeO_2-ZrO_2 catalysts prepared by a single-step sol-gel method: effect of acidity and basicity of the catalysts, Korean J. Chem. Eng. 29 (2012) 1019–1024, https://doi.org/10.1007/s11814-012-0017-0.

[37] P. Kumar, P. With, V.C. Srivastava, R. Glaser, I.M. Mishra, Conversion of carbon dioxide along with methanol to dimethyl carbonate over ceria catalyst, J. Environ. Chem. Eng. 3 (2015) 2943–2947, https://doi.org/10.1016/j.jece.2015.10.016.

[38] S.P. Wang, L.F. Zhao, W. Wang, Y.J. Zhao, G.L. Zhang, X.B. Ma, J.L. Gong, Morphology control of ceria nanocrystals for catalytic conversion of CO_2 with methanol, Nanoscale 5 (2013) 5582–5588, https://doi.org/10.1039/c3nr00831b.

[39] S.Y. Zhao, S.P. Wang, Y.J. Zhao, X.B. Ma, An in situ infrared study of dimethyl carbonate synthesis from carbon dioxide and methanol over well-shaped CeO_2, Chin. Chem. Lett. 28 (2017) 65–69, https://doi.org/10.1016/j.cclet.2016.06.003.

[40] B. Liu, C.M. Li, G.Q. Zhang, X.S. Yao, S.S.C. Chuang, Z. Li, Oxygen vacancy promoting dimethyl carbonate synthesis from CO_2 and methanol over Zr-doped CeO_2 nanorods, ACS Catal. 8 (2018) 10446–10456, https://doi.org/10.1021/acscatal.8b00415.

[41] Z.W. Fu, Y.H. Yu, Z. Li, D.M. Han, S.J. Wang, M. Xiao, Y.Z. Meng, Surface reduced CeO_2 nanowires for direct conversion of CO_2 and methanol to dimethyl carbonate: catalytic performance and role of oxygen vacancy, Catalysts 8 (2018) 164, https://doi.org/10.3390/catal8040164.

[42] W.F. Kuan, C.H. Chung, M.M. Lin, F.Y. Tu, Y.H. Chen, W.Y. Yu, Activation of carbon dioxide with surface oxygen vacancy of ceria catalyst: an insight from in-situ X-ray absorption near edge structure analysis, Mater. Today Sustain. 23 (2023) 100425, https://doi.org/10.1016/j.mtsust.2023.100425.

[43] C.T. Campbell, C.H.F. Peden, Chemistry - oxygen vacancies and catalysis on ceria surfaces, Science 309 (2005) 713–714, https://doi.org/10.1126/science.1113955.

[44] S. Wada, K. Oka, K. Watanabe, Y. Izumi, Catalytic conversion of carbon dioxide into dimethyl carbonate using reduced copper-cerium oxide catalysts as low as 353 K and 1.3 MPa and the reaction mechanism, Frontiers Chem. 1 (2013) 8, https://doi.org/10.3389/fchem.2013.00008.

[45] S.W. Yang, H.D. Shen, F. Cheng, C. Wu, Y.L. Cao, S.F. Zhuo, Q.Y. Zhang, H. P. Zhang, Organometallic precursor induced defect-enriched mesoporous CeO_2 with high specific surface area: preparation and catalytic performance, J. Mater. Chem. A 8 (2020) 14006–14014, https://doi.org/10.1039/d0ta02218g.

[46] Z.W. Fu, Y.Y. Zhong, Y.H. Yu, L.Z. Long, M. Xiao, D.M. Han, S.J. Wang, Y.Z. Meng, TiO_2-doped CeO_2 nanorod catalyst for direct conversion of CO_2 and CH_3OH to dimethyl carbonate: catalytic performance and kinetic study, ACS Omega 3 (2018) 198–207, https://doi.org/10.1021/acsomega.7b01475.

[47] C. Daniel, Y. Schuurman, D. Farrusseng, Surface effect of nano-sized cerium-zirconium oxides for the catalytic conversion of methanol and CO_2 into dimethyl carbonate, J. Catal. 394 (2021) 486–494, https://doi.org/10.1016/j.jcat.2020.09.023.

[48] P. Kumar, L. Matoh, R. Kaur, U.L. Stangar, Synergic effect of manganese oxide on ceria based catalyst for direct conversion of CO_2 to green fuel additive: catalyst activity and thermodynamics study, Fuel 285 (2021) 119083, https://doi.org/10.1016/j.fuel.2020.119083.

[49] Y.D. Chen, Y. Li, W. Chen, W.W. Xu, Z.K. Han, A. Waheed, Z.B. Ye, G. Li, A. Baiker, Continuous dimethyl carbonate synthesis from CO_2 and methanol over $Bi_xCe_{1-x}O$ delta monoliths: effect of bismuth doping on population of oxygen vacancies, activity, and reaction pathway, Nano Res. 15 (2022) 1366–1374, https://doi.org/10.1007/s12274-021-3669-4.

[50] K. Tomishige, Y. Ikeda, T. Sakaihori, K. Fujimoto, Catalytic properties and structure of zirconia catalysts for direct synthesis of dimethyl carbonate from methanol and carbon dioxide, J. Catal. 192 (2000) 355–362, https://doi.org/10.1006/jcat.2000.2854.

[51] Z.F. Zhang, Z.T. Liu, Z.W. Liu, J. Lu, DMC formation over $Ce_{0.5}Zr_{0.5}O_2$ prepared by complex-decomposition method, Catal. Lett. 129 (2009) 428–436, https://doi.org/10.1007/s10562-008-9816-7.

[52] K. Tomishige, Y. Furusawa, Y. Ikeda, M. Asadullah, K. Fujimoto, CeO_2-ZrO_2 solid solution catalyst for selective synthesis of dimethyl carbonate from methanol and carbon dioxide, Catal. Lett. 76 (2001) 71–74, https://doi.org/10.1023/a:1016711722721.

[53] R. Saada, S. Kellici, T. Heil, D. Morgan, B. Saha, Greener synthesis of dimethyl carbonate using a novel ceria-zirconia oxide/graphene nanocomposite catalyst, Appl. Catal. B 168 (2015) 353–362, https://doi.org/10.1016/j.apcatb.2014.12.013.

[54] P. Kumar, P. With, V.C. Srivastava, K. Shukla, R. Glaser, I.M. Mishra, Dimethyl carbonate synthesis from carbon dioxide using ceria-zirconia catalysts prepared using a templating method: characterization, parametric optimization and chemical equilibrium modeling, RSC Adv. 6 (2016) 110235–110246, https://doi.org/10.1039/c6ra22643d.

[55] G.L. Zhou, H.R. Liu, K.K. Cui, A.P. Jia, G.S. Hu, Z.J. Jiao, Y.Q. Liu, X.M. Zhang, Role of surface ni and ce species of Ni/CeO_2 catalyst in CO_2 methanation, Appl. Surf. Sci. 383 (2016) 248–252, https://doi.org/10.1016/j.apsusc.2016.04.180.

[56] G.Q. Zhang, Y. Zhou, Y.L. Yang, T.T. Kong, Y. Song, S. Zhang, H.Y. Zheng, Elucidating the role of surface Ce^{4+} and oxygen vacancies of CeO_2 in the direct synthesis of dimethyl carbonate from CO_2 and methanol, Molecules 28 (2023) 3785, https://doi.org/10.3390/molecules28093785.

[57] M. Lammert, M.T. Wharmby, S. Smolders, B. Bueken, A. Lieb, K.A. Lomachenko, D. De Vos, N. Stock, Cerium-based metal organic frameworks with UiO-66 architecture: synthesis, properties and redox catalytic activity, Chem. Commun. 51 (2015) 12578–12581, https://doi.org/10.1039/c5cc02606g.

[58] Z.J. Gong, Y.R. Li, H.L. Wu, S.D. Lin, W.Y. Yu, Direct copolymerization of carbon dioxide and 1,4-butanediol enhanced by ceria nanorod catalyst, Appl. Catal. B 265 (2020) 118524, https://doi.org/10.1016/j.apcatb.2019.118524.

[59] Y.H. Wang, C.H. Chuang, T.A. Chiu, C.W. Kung, W.Y. Yu, Size-tunable synthesis of palladium nanoparticles confined within topologically distinct metal-organic frameworks for catalytic dehydrogenation of methanol, J. Phys. Chem. C 124 (2020) 12521–12530, https://doi.org/10.1021/acs.jpcc.0c02743.

[60] Z.J. Gong, C.C. Chien, S. Mudhulu, J.C.S. Wu, N. Daneu, M.M. Krzmanc, W.Y. Yu, $SrTiO_3$ catalysts prepared from topochemical conversion of $Bi_4Ti_3O_{12}$ nanoplatelets: surface characterizations and interactions with isopropanol, J. Catal. 416 (2022) 222–232, https://doi.org/10.1016/j.jcat.2022.11.001.

[61] F.H. Hu, L.T. Chi, G.B. Syu, T.Y. Yu, M.P. Lin, J.J. Chen, W.Y. Yua, D.Y. Kang, Mixed-linker MOF-303 membranes for pervaporation, J. Membr. Sci. Lett. 3 (2023) 100053, https://doi.org/10.1016/j.memlet.2023.100053.

[62] Z.L. Wu, M.J. Li, J. Howe, H.M. Meyer, S.H. Overbury, Probing defect sites on CeO_2 nanocrystals with well-defined surface planes by raman spectroscopy and O_2 adsorption, Langmuir 26 (2010) 16595–16606, https://doi.org/10.1021/la101723w.

[63] T. Taniguchi, T. Watanabe, N. Sugiyama, A.K. Subramani, H. Wagata, N. Matsushita, M. Yoshimura, Identifying defects in ceria-based nanocrystals by UV resonance raman spectroscopy, J. Phys. Chem. C 113 (2009) 19789–19793, https://doi.org/10.1021/jp9049457.

[64] R.H. Gao, D.S. Zhang, P. Maitarad, L.Y. Shi, T. Rungrotmongkol, H.R. Li, J. P. Zhang, W.G. Cao, Morphology-dependent properties of MnO_x/ZrO_2-CeO_2 nanostructures for the selective catalytic reduction of NO with NH_3, J. Phys. Chem. C 117 (2013) 10502–10511, https://doi.org/10.1021/jp400984z.

[65] F. Larachi, J. Pierre, A. Adnot, A. Bernis, Ce 3d XPS study of composite $Ce_xMn_{1-x}O_{2-y}$ wet oxidation catalysts, Appl. Surf. Sci. 195 (2002) 236–250, https://doi.org/10.1016/s0169-4332(02)00559-7.

[66] H. Liu, W.J. Zou, X.L. Xu, X.L. Zhang, Y.Q. Yang, H.J. Yue, Y. Yu, G. Tian, S. H. Feng, The proportion of Ce^{4+} in surface of $CexZr_{1-x}O_2$ catalysts: the key parameter for direct carboxylation of methanol to dimethyl carbonate, J. CO_2 Util. 17 (2017) 43–49, https://doi.org/10.1016/j.jcou.2016.11.006.

[67] H.C. Yao, Y.F.Y. Yao, Ceria in automotive exhaust catalysts I. oxygen storage, J. Catal. 86 (1984) 254–265, https://doi.org/10.1016/0021-9517(84)90371-3.

[68] C.Z. Zhu, X.Q. Wei, W.Q. Li, Y. Pu, J.F. Sun, K.L. Tang, H.Q. Wan, C.Y. Ge, W. X. Zou, L. Dong, Crystal-plane effects of CeO_2 {110} and CeO_2 {100} on photocatalytic CO_2 reduction: synergistic interactions, of oxygen defects and hydroxyl groups, ACS Sustain. Chem. Eng. 8 (2020) 14397–14406, https://doi.org/10.1021/acssuschemeng.0c04205.

[69] I. Prymak, V.N. Kalevaru, S. Wohlrab, A. Martin, Continuous synthesis of diethyl carbonate from ethanol and CO_2 over Ce-Zr-O catalysts,, Catal. Sci. Technol. 5 (2015) 2322–2331, https://doi.org/10.1039/c4cy01400f.

[70] Z.Q. Wang, M.J. Zhang, X.B. Hu, V.P. Dravid, Z.N. Xu, G.C. Guo, CeO_{2-x} quantum dots with massive oxygen vacancies as efficient catalysts for the synthesis of dimethyl carbonate, Chem. Commun. 56 (2020) 403–406, https://doi.org/10.1039/c9cc07584d.

[71] M. Capdevila-Cortada, G. Vile, D. Teschner, J. Perez-Ramirez, N. Lopez, Reactivity descriptors for ceria in catalysis, Appl. Catal. B 197 (2016) 299–312, https://doi.org/10.1016/j.apcatb.2016.02.035.

[72] J.C. Conesa, Computer modeling of surfaces and defects on cerium dioxide, Surf. Sci. 339 (1995) 337–352, https://doi.org/10.1016/0039-6028(95)00595-1.

[73] H. Cordatos, D. Ford, R.J. Gorte, Simulated annealing study of the structure and reducibility in ceria clusters, J. Phys. Chem. C 100 (1996) 18128–18132, https://doi.org/10.1021/jp961110o.

[74] T.X.T. Sayle, S.C. Parker, C.R.A. Catlow, The role of oxygen vacancies on ceria surfaces in the oxidation of carbon-monoxide, Surf. Sci. 316 (1994) 329–336, https://doi.org/10.1016/0039-6028(94)91225-4.

[75] X.W. Liu, K.B. Zhou, L. Wang, B.Y. Wang, Y.D. Li, Oxygen vacancy clusters promoting reducibility and activity of ceria nanorods, J. Am. Chem. Soc. 131 (2009) 3140–3141, https://doi.org/10.1021/ja808433d.

[76] S.D. Senanayake, W.O. Gordon, S.H. Overbury, D.R. Mullins, Adsorption and reaction of acetone over CeO_x (111) thin films, J. Phys. Chem. C 113 (2009) 6208–6214, https://doi.org/10.1021/jp810403d.

[77] S. Rousseau, O. Marie, P. Bazin, M. Daturi, S. Verdier, V. Harle, Investigation of methanol oxidation over Au/catalysts using operando IR spectroscopy: determination of the active sites, intermediate/spectator species, and reaction mechanism, J. Am. Chem. Soc. 132 (2010) 10832–10841, https://doi.org/10.1021/ja1028809.

[78] M. Honda, M. Tamura, Y. Nakagawa, K. Nakao, K. Suzuki, K. Tomishige, Organic carbonate synthesis from CO_2 and alcohol over CeO_2 with 2-cyanopyridine: scope and mechanistic studies, J. Catal. 318 (2014) 95–107, https://doi.org/10.1016/j.jcat.2014.07.022.